Effect of Nanowire Number, Diameter, and Doping Density on Nano-FET Biosensor Sensitivity

Jason Li,[†,‡,⊥] Yanliang Zhang,[†,⊥] Steve To,[§] Lidan You,[†,‡,*] and Yu Sun[†,‡,§,*]

[†]Department of Mechanical and Industrial Engineering, [‡]Institute of Biomaterials and Biomedical Engineering, and [§]Department of Electrical and Computer Engineering, University of Toronto, Toronto ON M5S 3G8, Canada [⊥]These authors contributed equally to this work.

ABSTRACT Semiconductive nanowire-based biosensors are capable of label-free detection of biological molecules. Nano-FET (field-effect transistor) biosensors exhibiting high sensitivities toward proteins, nucleic acids, and viruses have been demonstrated. Rational device design methodologies, particularly those based on theoretical predictions, were reported. However, few experimental studies have investigated the effect of nanowire diameter, doping density, and number on nano-FET sensitivity. In this study, we devised a fabrication process based on parallel approaches and nanomanipulation-based post-processing for constructing nano-FET biosensor devices with carefully controlled nanowire parameters (diameter, doping density, and number). We experimentally reveal the effect of these nanowire parameters on nano-FET biosensor sensitivity. The experimental findings quantitatively demonstrate that device sensitivity decreases with increasing number of nanowires (4 and 7 nanowire devices exhibited a ~38 and ~82% decrease in sensitivity as compared to a single-nanowire device), larger nanowire diameters (sensors with 81−100 and 101−120 nm nanowire diameters exhibited a ~16 and ~37% decrease in sensitivity compared to devices with nanowire diameters of 60−80 nm), and higher nanowire doping densities (~69% decrease in sensitivity due to an increase in nanowire doping density from 10^{17} to 10^{19} atoms · cm^{-3}). These results provide insight into the importance of controlling nanowire properties for maximizing sensitivity and minimizing performance variation across devices when designing and manufacturing nano-FET biosensors.

KEYWORDS: nano-FET · biosensor · nanowire number · nanowire diameter · nanowire doping density · nanomanipulation · nano-FET fabrication

Nanowire field-effect transistors (nano-FETs) enable dynamic label-free detection of molecules with higher sensitivity and shorter detection times compared to conventional bioassays. Research efforts over the past decade have produced significant advances in nano-FET biosensor technology and resulted in highly sensitive proof-of-concept devices capable of detecting exceedingly low concentrations of proteins,[1−3] nucleic acids,[4,5] and viruses[6] in solution. In order to achieve high performance and consistency across devices, understanding sensing mechanisms and the effect of important parameters is important. A number of experimental studies have been reported, which sought to elucidate the sensing mechanism and the effect of various device parameters on nano-FET sensitivity including electrode material,[7] nanowire composition,[8,9] functionalization method, receptor size,[10,11] gate bias,[12−14] electrolyte ion concentration,[15,16] and analyte delivery methods.[17−19] However, the influence of *nanowire number*, *doping density*, and *diameter* on nano-FET biosensor sensitivity remains to be experimentally quantified.

Previous studies explored the influence of nanowire number, doping density, and diameter on device sensitivity in the context of nanowire electrical transport studies,[20−22] gas-phase chemical sensing,[8,23] aqueous sensing of pH and ionic species,[3,24] and nanoribbon FETs.[25,26] However, fundamental differences between these sensor systems and nanowire FET biosensors require that the effect of these parameters be experimentally examined under biomolecule sensing conditions to obtain quantitatively meaningful relationships. Several numerical models were also established for qualitatively predicting nano-FET biosensor sensitivity dependence on nanowire diameter, doping concentration, and number.[12,27,28]

Herein we experimentally determine the influence of nanowire number (the number of bridging nanowires incorporated into each device), nanowire doping density, and nanowire diameter on the sensitivity of silicon nanowire FET protein sensors using human immunoglobulin G (hIgG) as a model analyte. As existing large-scale nano-FET construction methods such as directed self-assembly,[29−31] contact printing,[32−34] flow alignment,[35] and dielectrophoresis[36,37] of presynthesized nanostructures are incapable of precisely controlling the diameter and/or number of nanowires incorporated into each device, we further present a unique fabrication method to achieve reliable nanowire number and diameter control through a combined use of

* Address correspondence to sun@mie.utoronto.ca, youlidan@mie.utoronto.ca.

Received for review June 14, 2011 and accepted July 26, 2011.

Published online August 04, 2011
10.1021/nn202182p

existing large-scale nanowire integration methods and post-processing using nanomanipulation inside a scanning electron microscope (SEM). This process is different from existing top-down micro- and nanofabrication techniques for nanowire production (*e.g.*, electron-beam nanolithography,[1] silicon wire thinning *via* repeated surface oxidation and HF etching processes,[25,38] and anisotropic timed etching of silicon structures[3]), which involve high processing costs and low yields associated with e-beam lithography, and significant variability across etched devices due to etching non-uniformity across wafer and high sensitivity to processing conditions. Using this technique, we are able to fabricate arrays of nano-FET biosensors in a reliable manner with carefully controlled nanowire properties for subsequent investigation of their effects on device sensitivity.

RESULTS AND DISCUSSION

Nanomanipulation for the Fabrication of Nano-FET Devices. In conjunction with conventional microfabrication methods, wafer-scale fabrication of nano-FET biosensors was previously made possible by several large-scale nanowire-positioning techniques such as flow alignment[35] and contact printing[32] of presynthesized nanowires. Devices fabricated in this manner consist of numerous nanowires, orientated parallel with one another along a direction, bridging the source−drain electrode pair (Figure 1a). In addition, the effective length of each nanowire is dictated by the electrode pair gap size. Although efficient, drawbacks of this approach include the inability to reliably control the number and diameters of incorporated nanowires within each device. Additional post-processing procedures may therefore be useful for controlling device parameters such as nanowire number and diameter. We first explored the use of focused ion beam (FIB) milling for selective nanowire removal. However, as previously reported by Hu *et al.*,[39] EDX (energy-dispersive X-ray spectroscopy) analysis of FIB-milled samples revealed substantial deposition and/or implantation of gallium atoms around the milled region (Figure 2). Due to the concern of gallium contamination on silicon nanowires, an effect that has been previously demonstrated to strongly alter the nanowires' charge transport properties (at typical FIB Ga+ fluences of 30 keV),[40] we chose physical nanomanipulation for this nano-FET characterization study.

Physical nanomanipulation, despite being slower compared to the large-scale methods, promises specificity, precision, and programmed motion and, thus, enables the manipulation and characterization of individual nanowires. We demonstrate the use of a nanomanipulation post-processing method to selectively remove unwanted nanowires from multinanowire devices to form nano-FET biosensors with well-controlled number of nanowires and nanowire diameters (Figure 1). The number of nanowires per device and their respective diameters were controlled using a piezoelectric nanomanipulator inside an SEM (Figure 1b). A substrate with multinanowire transistor arrays was loaded into the SEM equipped with a nanomanipulation system with nanometer motion resolutions. The system determines diameters of each bridging nanowire *via* imaging processing and also identifies nanowire(s) of interest (those to retain and remove). Tungsten nanoprobes were then brought into close proximity of the nano-FET devices and placed into contact with the substrate. Unwanted bridging nanowires were physically severed and removed by running the nanoprobes along the electrode edges across the nanowire(s) (Figure 1c−e). Pinning of the nanowires beneath the contact electrodes caused the nanowire to break precisely at the electrode edges. Positioning of nanoprobes with nanometer resolution enabled the removal of individual nanowires without disturbing adjacent nanowires. Automation of this process facilitated the manufacturing of single- or multiple-nanowire transistors in a reproducible manner at a speed of ∼1 min per device. Using this method, the fabrication yield is in excess of ∼95% with a ∼5% failure rate that is attributed to (1) insufficient number of nanowire(s) of the desired diameter/orientation that bridge the electrode gap, (2) accidental severing of desired nanowire(s) during nanomanipulation, or (3) erroneous identification of bridging nanowire parameters *via* automated image analysis (*e.g.*, failure to identify two nanowires lying on top of each other as such). It should be noted that these yields are dependent on the quality of the nanowire contact-printing process as well as the density and quality of nanowires on the donor substrate.

Electrical characterization was subsequently performed to obtain device $I-V$ characteristics and to verify Ohmic nanowire−electrode contact, the intactness of the thermal oxide layer, and proper n-type FET electrical characteristics (Figure 1f). Electrical testing further confirmed that all devices had stable signals. For single-nanowire devices, this indicates that each bridging nanowire in physical contact with the electrodes was indeed conductive. Although it is difficult to determine if the same is true for multinanowire devices, based on the results for single-nanowire devices, we trust that the overwhelming majority of bridging nanowires in the multinanowire devices are also conductive. All nanowires, nanowire−electrode junctions, and electrodes were inspected for cracks and defects using high-magnification SEM imaging. No cracks or surface defects were observed in the nanowires or nanowire−electrode junctions. No new defects were observed in the electrodes as a result of nanomanipulation post-processing. Testing of 10 single-nanowire transistor devices (V_{sd} = 10 mV, V_g = 0 V) fabricated using the same batch of nanowires (10^{19} atoms/cm^3)

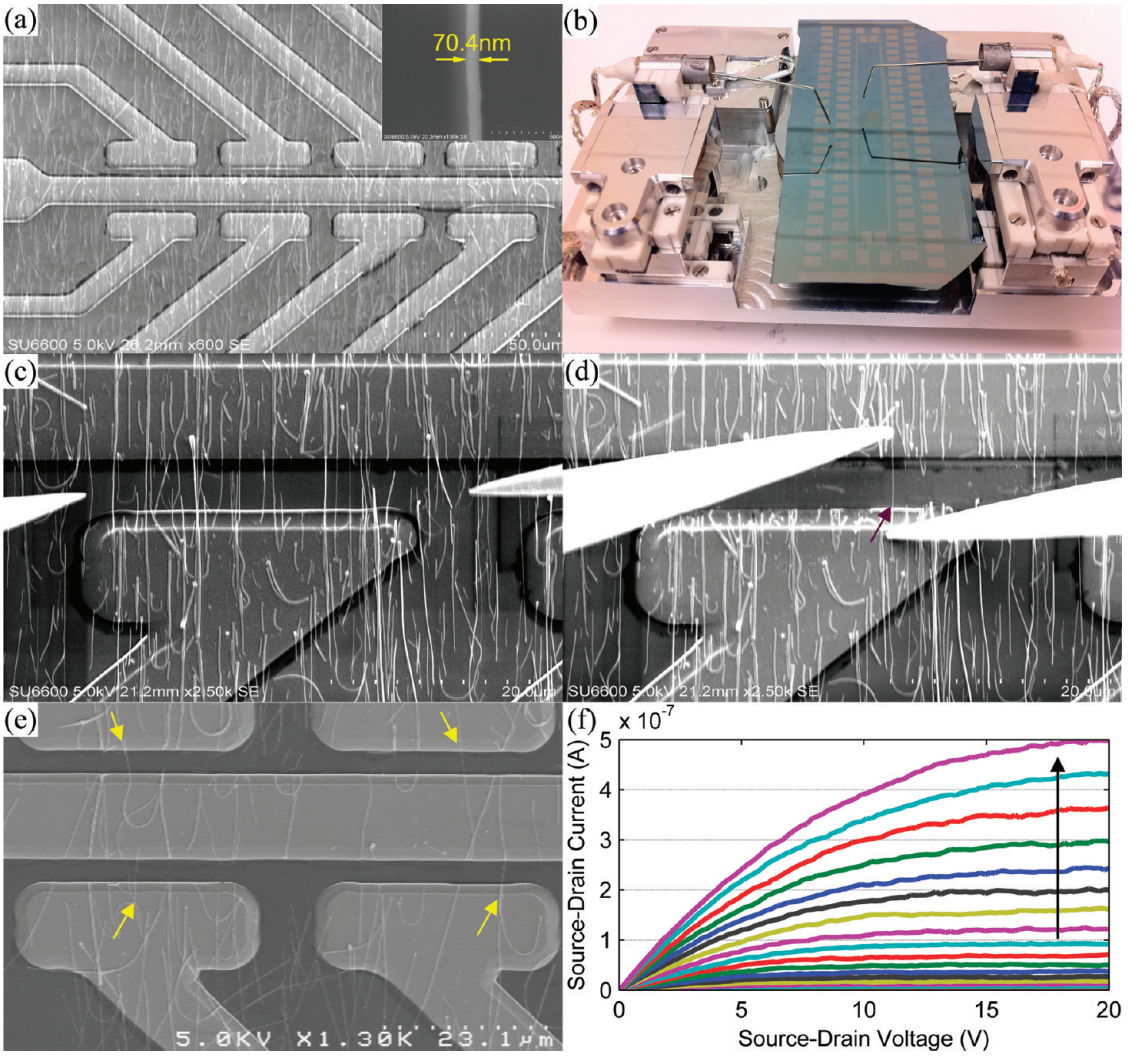

Figure 1. Nanowire FET construction. (a) Batch fabricated device arrays using contact printing and standard photolithography, metallization, and lift-off (8 source electrodes and 1 common drain electrode shown). Devices have multiple nanowires of various diameters bridging microelectrodes. The microelectrodes are on top of nanowires and pin the nanowires down on the substrate. Inset: high-magnification (100 000×) SEM image of a single nanowire section. (b) Batch fabricated nano-FET array mounted on an SEM stage for nanomanipulation (nanowire selection and nanowire removal). (c,d) Before and after nanomanipulation removal of nanowires between the source and drain electrodes (arrow: retained single nanowire). (e) Array of 4 single-nanowire devices (arrows: remaining nanowire). (f) Current−voltage characteristics of a post-processed nanowire FET device (V_{sd} = 0 to +20 V, $V_{backgate}$ = −25 to +25 V, increasing $V_{backgate}$ indicated by arrow).

exhibited an average conductance of 1.06×10^{-7} S and a variance of 2.30×10^{-15} S ($\sigma = 4.79 \times 10^{-8}$). Variation in device conductance may be attributed to slight differences in nanowire properties (diameter, doping concentration, imperfections) and small differences in the contacting electrode lengths between devices.

Sensitivity Dependence on Nanowire Number. We first examined the effect of nanowire number on nano-FET biosensing sensitivity. Previous studies have suggested that the number of bridging nanowires incorporated into a device may be an important parameter in determining sensitivity.[23,41] Zhang *et al.*[23] demonstrated that multiple In_2O_3 nanowire FET devices were more sensitive than single-nanowire devices for gaseous chemical sensing. While the underlying mechanism was not determined, the authors speculated that this observation might be attributed to the formation of nanowire−nanowire junctions between overlapping nanowires. Gruner *et al.*[41] further suggested that individual carbon nanotube (CNT) FET biosensors, as compared to CNT network devices, exhibited higher sensitivity. As these sensing systems differ from nano-FET biosensors in terms of sensing environment, molecule of interest, and/or nanostructure composition and type, herein we investigate the dependence of nanowire number in nanowire-based biological sensing. Twelve devices with exactly 1, 4, or 7 bridging nanowires (80−100 nm diameter; 4 devices each) were fabricated and characterized in response to increasing concentrations of hIgG (Figure 3a,b). All sensors exhibited linear relationships between source−drain current (I) and log[hIgG].[28] Device sensitivity, defined as $(I - I_0)/I_0$, was found to be maximal for single-nanowire

devices (0.05 per decade; n = 4) and decreased for increasing number of nanowires (0.031 per decade for 4 nanowires and 0.009 per decade for 7 nanowires, which represents a ~38 and ~82% decrease in sensitivity, respectively; n = 4 for each case), suggesting that single-nanowire devices can yield the highest sensitivity.

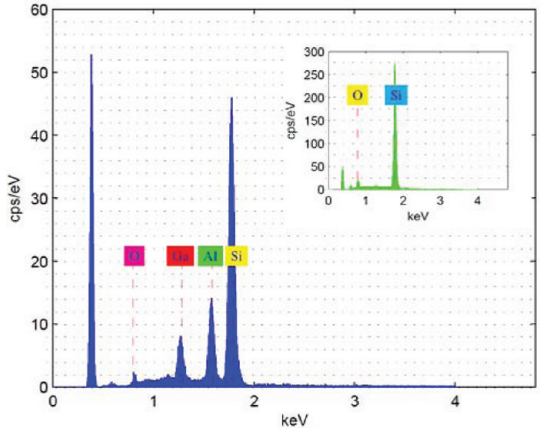

Figure 2. EDX analysis of a device with nanowires removed with focused ion beam (FIB) milling. Ga atoms are present in the proximity of the milled region. Inset: EDX analysis of a region away from the milled region with no presence of Ga atoms.

As no nanowire−nanowire junctions were present in our devices, we attribute this phenomenon to the depletion of hIgG molecules from solution around the nanowires. For a single-nanowire device, which experiences an initial source−drain current of $I_{0(1nw)}$, introducing analyte solution results in the binding of x_{1nw} molecules onto the nanowire surface to produce a change in device current $(I - I_0)_{1nw}$, and the sensitivity is $(I - I_0)_{1nw}/I_{0(1nw)}$. Similarly, for a multinanowire device (n nanowires connected in parallel) with an initial source−drain current of $I_{0\ (n\ \text{nanowires})} = n \times I_{0(1nw)}$, if we assume that there is no appreciable depletion of analyte molecules from solution, then a total current change of $(I - I_0)_{(n\ \text{nanowires})} = n \times (I - I_0)_{1nw}$ would be expected. Under this assumption, the sensitivity of a nano-FET sensor with n parallel nanowires is then $(I - I_0)_{(n\ \text{nanowires})}/I_{0(n\ \text{nanowires})} = n(I - I_0)_{1nw}/nI_{0(1nw)} = (I - I_0)_{1nw}/I_{0(1nw)}$, which is equivalent to that of a single-nanowire device. However, for low concentrations of analyte, a finite number of analyte molecules are located in the immediate vicinity around

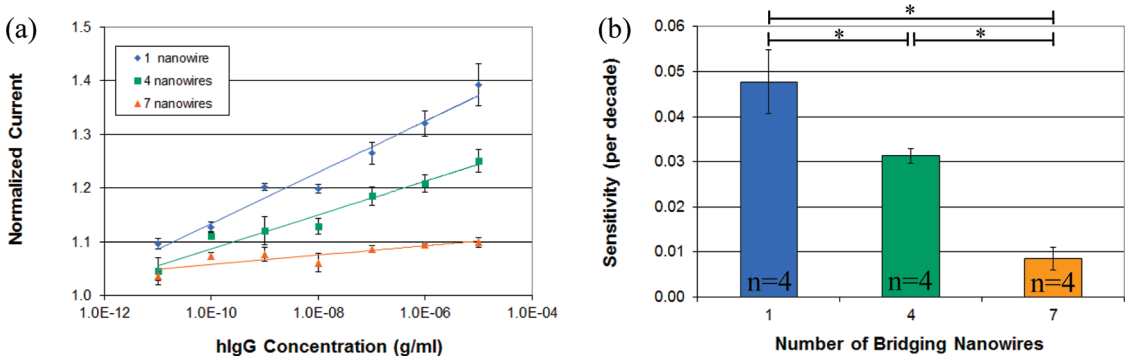

Figure 3. Effect of nanowire number on device sensitivity. (a) Normalized current as a function of protein concentration for devices with 1, 4, and 7 nanowires (n = 4 for each group; nanowire diameter = 81−100 nm; nanowire doping density = 10^{19} atoms·cm^{-3}). (b) Sensitivity as a function of the number of bridging nanowires (n = 4 for each group). Decreasing sensitivity was observed for higher numbers of nanowires (n = 4 for each group; *p < 0.05).

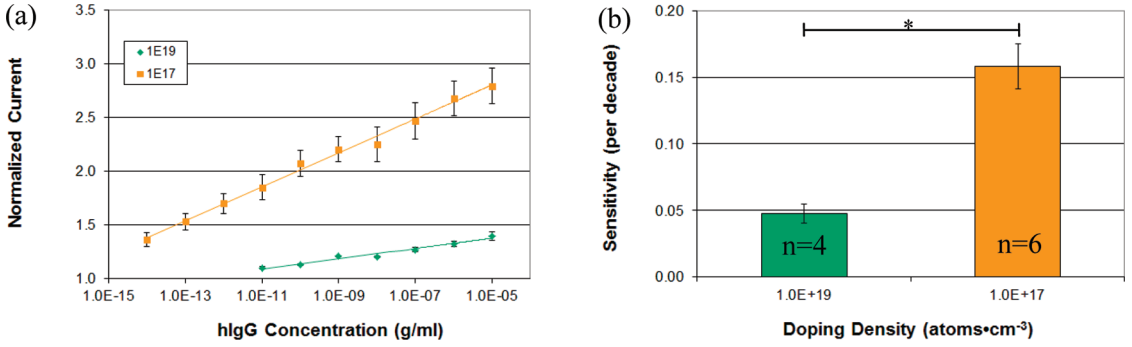

Figure 4. Effect of nanowire doping concentration on device sensitivity. (a) Normalized current as a function of protein concentration for single-nanowire devices with a nanowire doping density of either 10^{19} or 10^{17} atoms·cm^{-3}. All devices (n = 4 and n = 6 for experimental groups with doping densities of 10^{19} or 10^{17} atoms·cm^{-3}, respectively) contained only a single nanowire (diameter = 81−100 nm). A lower nanowire doping density resulted in devices of higher sensitivity and also with a significantly improved detection limit (~10 fg/mL *vs* ~10 pg/mL). (b) A ~3.2-fold increase in sensitivity was observed corresponding to the 2 order of magnitude decrease in nanowire doping density ($n \geq 4$ for each group; *p < 0.05).

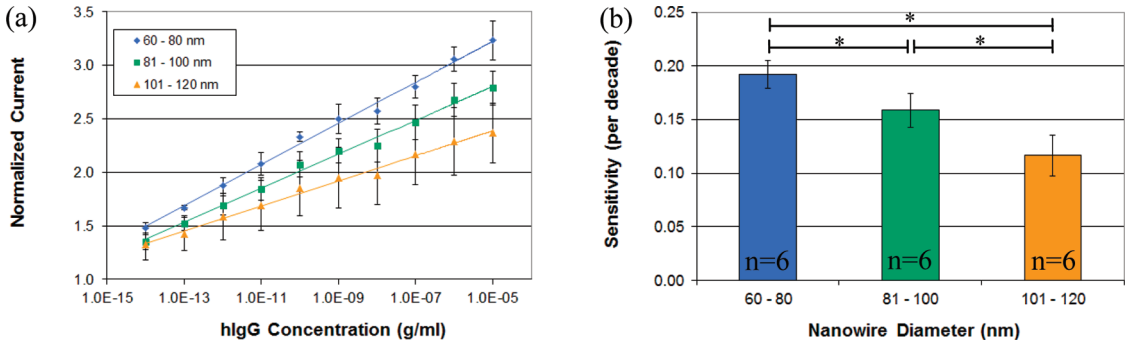

Figure 5. Effect of nanowire diameter on device sensitivity. Single-nanowire devices with diameters ranging between 60 and 120 nm were characterized. Nanowire diameters were grouped into three categories: 60−80, 81−100, and 101−120 nm. Nanowire doping densities were 10^{17} atoms·cm^{-3}. (a) Normalized current as a function of protein concentration for single-nanowire devices with different nanowire diameters (n = 6 for each group). (b) Smaller nanowire diameters produced more sensitive nanowire FET biosensors (n = 6 for each group; *p < 0.05).

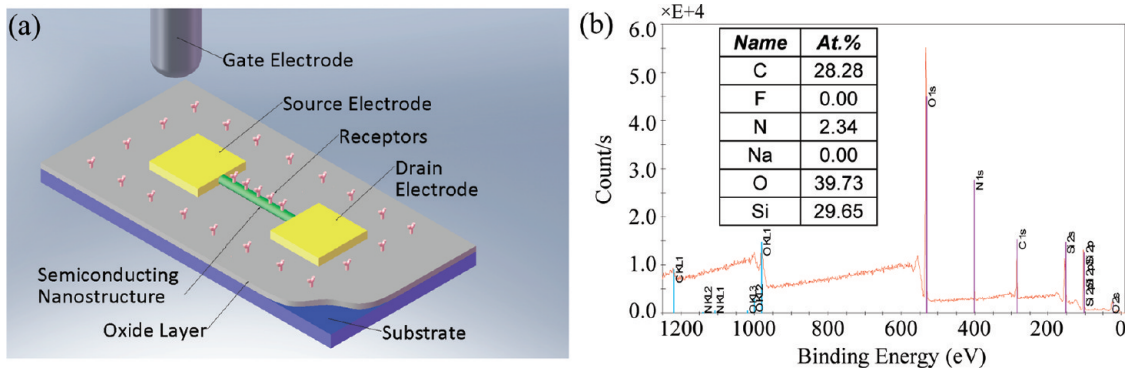

Figure 6. (a) Schematic of a single-nanowire FET biosensor after biofunctionalization (b) XPS analysis verifies successful conjugation of APTES molecules, as indicated by the presence of nitrogen.

the nano-FET device. Therefore, the effect of analyte depletion from the surrounding solution becomes significant[17,19] and effectively decreases the number of nanowire−analyte binding events experienced per nanowire. Thus, for a multinanowire FET device in which multiple closely spaced nanowires compete for the binding of free analyte molecules, the number of nanowire−analyte interactions for each nanowire is expected to decrease for increasing numbers of nanowires such that $x_{(n\ \text{nanowires})} < x_{1\text{nw}}$, resulting in a smaller current change for each nanowire. Therefore, a lower sensitivity is expected for nano-FET devices with multiple nanowires (*i.e.*, $(I - I_0)_{(n\ \text{nanowires})}/I_{0(n\ \text{nanowires})} < (I - I_0)_{1\text{nw}}/I_{0(1\text{nw})}$). While further testing is required to conclude that analyte depletion is indeed the cause for the experimental observations, the results indicate that precise control over the number of bridging nanowires incorporated into a nano-FET device is important to optimizing device sensitivity, and that the control of nanowire spacing in multinanowire sensors may have practical implications.

Sensitivity Dependence on Nanowire Doping. We next examined the effect of nanowire doping concentration on nano-FET sensitivity. Single-nanowire devices, with diameters between 80 and 100 nm, were constructed using nanowires of two different doping concentrations (10^{17} and 10^{19} atoms/cm^3, n = 6 and n = 4 respectively). Source−drain current was measured as increasing concentrations of hIgG solution (10 fg/mL to 10 μg/mL) were introduced to the sensor surface. Nano-FET sensitivity was extracted as a function of protein concentration and correlated with the nanowire doping concentration. Figure 4 shows that a 2 order of magnitude change in doping concentration (from 10^{19} to 10^{17} atoms·cm^{-3}) resulted in a ~3.2-fold increase in nano-FET sensitivity from 0.05 to 0.16 per decade. The sensitivity increase was also accompanied by a significantly lower sensor detection limit (~10 fg/mL *vs* ~10 pg/mL) for hIgG.

These results reveal that nano-FET sensitivity is strongly dependent on nanowire doping concentration, with lower doping densities resulting in higher device sensitivity. These findings are in qualitative agreement with computational modeling predictions.[27] However, direct quantitative comparisons cannot be made due to differences in nanowire dimensions used in the present study and previous studies. As previously reported in the literature, this observation may be attributed to the reduced effect of charge screening by mobile charge carriers in nanowires with lower doping densities.[27]

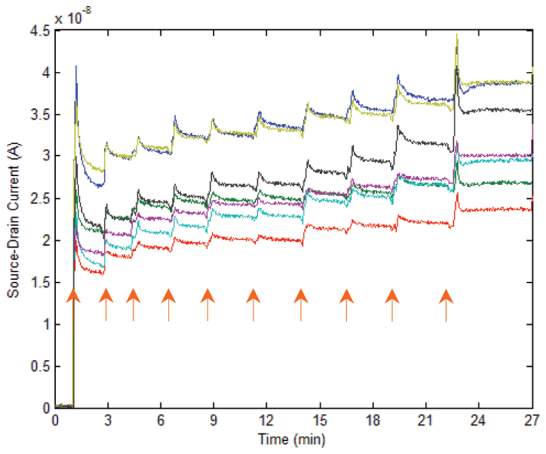

Figure 7. Typical current−time response for 7 Si nanowire FET biosensors. Device current increased from a baseline value (dry device) upon subsequent addition of sample solution with increasing concentrations of hIgG in 0.1× PBS buffer (from 10 fg/mL to 10 μg/mL). Arrows indicate additions of sample solution.

Sensitivity Dependence on Nanowire Diameter. We finally investigated the effect of nanowire diameter on nano-FET sensitivity. While several nano-FET gas[8] and pH sensors[3,24] have demonstrated a sensitivity dependence on nanowire diameter, few experimental studies have examined this dependence for biosensing applications. Numerical modeling results of nanowire biosensors presented by Nair *et al.*[27] predicted a negative correlation between nanowire diameter and device sensitivity. However, the quantitative extent of this dependence has yet to be determined experimentally. We, therefore, explored the influence of nanowire diameter by fabricating single-nanowire devices with nanowire diameters ranging between 60 and 120 nm.

As diameter variations exist among presynthesized nanowires, we categorized our devices into three experimental groups based on their nanowire diameters: 60−80, 81−100, and 101−120 nm ($n = 6$ for each case). The sensors were then characterized against increasing concentrations of hIgG to determine device sensitivity. As shown in Figure 5, a negative relationship between nanowire diameter and device sensitivity was observed for single-nanowire devices with diameters ranging from 60 to 120 nm (0.12 to 0.19 per decade, ∼58% increase in sensitivity; $n = 6$), demonstrating that nano-FET devices with thinner nanowires exhibit a higher sensitivity. This trend is in agreement with the numerical modeling predictions reported by Nair *et al.*,[27] in agreement with experimental pH measurements made by Stern *et al.*,[42] and in agreement with nanoribbon-based FET (45−100 nm thick, 1 μm wide, 2 μm long) biosensing results observed by Elfstrom *et al.*[25]

Our results provide experimental evidence demonstrating the importance of control over nanowire properties in determining nano-FET biosensor sensitivity and further quantify the effect of three nano-FET biosensor parameters (nanowire number, doping density, and diameter) on device sensitivity. We are aware that when the effects of nanowire number and doping density were studied, there were slight variations in nanowire diameter (80−100 nm), which might introduce a parameter-coupling effect into the measurements. However, the potential coupling effect was captured and reflected in the variance of each measurement (standard deviation). The observed sensitivity change resulting from the intentional alteration of a single parameter was still statistically significant ($p < 0.05$) in all experiments.

CONCLUSIONS

In summary, we have demonstrated a fabrication method that combines large-scale fabrication and SEM nanomanipulation post-processing for constructing nano-FET biosensors relatively inexpensively with well-controlled nanowire number and diameters. Using this method, we constructed single-nanowire FET biosensors to experimentally study the effect of nanowire doping density and nanowire diameter on device sensitivity. We experimentally observed that nanowires with a lower doping density produce significantly more sensitive nano-FET sensors and that smaller nanowire diameters also improve device performance. Furthermore, we also experimentally demonstrated the effect of nanowire number on nano-FET biosensor sensitivity and have attributed the decreased sensitivity in multinanowire devices to competitive binding and depletion of analyte from the surrounding solution. This phenomenon further stipulates that separation distance between nanowires in a multiple-nanowire biosensor must be controlled in order to achieve device sensitivity comparable to single-nanowire devices. These findings may serve as a design reference for the optimization of nano-FET biosensor performance, in terms of both improving device sensitivity and minimizing variability across devices.

METHODS

Nanowire Synthesis. Phosphorus-doped (n-type) silicon nanowires (SiNWs) were synthesized on a silicon wafer growth substrate using a chemical vapor deposition (CVD) process *via* the gold-catalyzed vapor−liquid−solid nanowire growth mechanism (550 °C, 10−50 Torr, 10% SiH_4/H_2 silicon source, PH_3 dopant source; Illuminex Corp., USA). Nanowires synthesized under these conditions had a distribution of diameters between 60 and 120 nm. Two batches of nanowires with different doping concentrations (10^{17} and 10^{19} atoms/cm^3) were synthesized.

Fabrication of Nano-FET Arrays. Wafer-scale transfer of the as-grown nanowires onto a device substrate (degenerately doped silicon wafer with a 2000 nm thick thermal oxide layer) using the previously reported contact printing method[32] resulted in

the high-density deposition of well-aligned nanowires. Briefly, the growth substrate was inverted and placed on top of the device substrate such that the as-grown nanowires were sandwiched between the two silicon wafers. A weight was then placed above of the growth substrate to provide a normal force of 20 $g \cdot cm^{-2}$. Lateral displacement of the growth substrate over the device substrate at a constant velocity of 20 $mm \cdot min^{-1}$ resulted in the transfer of a high-density monolayer of well-aligned nanowires onto the device substrate. Standard photolithography, metallization, and lift-off wafer-level microfabrication processes were subsequently used to form 200 nm thick Al electrodes over the aligned nanowires producing arrays of multinanowire transistors (Figure 1a).

Integration with a Microfluidic System. After nanomanipulation post-processing to control nanowire number and diameter, nano-FET arrays were encapsulated into a simple microfluidic channel to facilitate easy solution handling during surface functionalization and subsequent biosensing experimentation. As the surface modification process functionalizes all oxide surfaces, incorporation of the microfluidic channel also served to restrict functionalization and fluid contact area during biosensing experiments. The microfluidic channels (5 mm $\times$ 1 mm $\times$ 0.4 mm) were fabricated by molding poly(dimethylsiloxane) (PDMS; Microchem Corp., Newton MA, USA) onto an SU-8 50 (Microchem Corp., USA) mold master using standard soft lithography. The channels were then detached from the mold master and irreversibly bonded onto the nano-FET arrays.

Nanowire Functionalization. Unless otherwise specified, all chemicals and reagents used for functionalization and biosensing experiments were purchased and used without further purification from Sigma-Aldrich (Oakville, Canada). Surface modification was performed using 2% (3-aminopropyl)triethoxysilane (APTES) in ethanol (30 min), 3% glutaraldehyde in phosphate buffered saline (0.01 M PBS, pH 7.4, 30 min), and anti-human IgG (Invitrogen, USA) in PBS.[43] Unreacted terminal aldehyde groups were passivated with a 100 mM ethanolamine solution in PBS (pH 8.4) and washed with a solution of 0.5% Tween-20 in PBS. Successful and repeatable functionalization of silicon oxide surfaces was verified using X-ray photon spectroscopy (XPS) and fluorescence microscopy analysis. Successful conjugation of APTES was verified by the presence of nitrogen atoms on the sample surface using XPS analysis (Figure 6). Immobilization of fluorescently tagged anti-hIgG (Alexa Fluor-488 anti-hIgG, Invitrogen) was verified using fluorescence microscopy.

Biosensing Experiments. All biosensing experiments were carried out at room temperature using various concentrations of hIgG in 0.1$\times$ PBS as a model analyte for immunodetection applications (Figure 7). The low ionic concentration of 0.1$\times$ was used to reduce the effect of charge screening by mobile ions in solution. Increasing concentrations of hIgG (from 10 $fg \cdot mL^{-1}$ up to 10 $\mu g \cdot mL^{-1}$) were introduced to the sensor surface, and sufficient time was given to ensure that signal equilibrium was reached before the addition of subsequent solutions. Electrical measurements were performed using a Keithley 2602 sourcemeter (for all biosensing experiments: $V_{sd} = 10$ mV, $V_g = -1.0$ V, I_{sd} was measured and recorded). The gate voltage was applied using a Ag/AgCl solution gate electrode immersed within the electrolyte.

Up to 18 devices were characterized simultaneously throughout experimentation using a LabVIEW-controlled data acquisition system and a multiplexer (National Instruments, USA). For each concentration of hIgG, the steady-state normalized device current (I/I_0) was measured and plotted against the protein concentration. Sensitivity, defined as $(I - I_0)/I_0$, was then determined and plotted against the test parameter. Statistical significance was determined using unpaired student t test assuming unequal variances ($p < 0.05$).

Acknowledgment. The authors acknowledge financial support from the Natural Sciences and Engineering Research Council of Canada, the Ontario Centres of Excellence, Hitachi High-Technologies Canada Inc., and the Canada Research Chairs program.

REFERENCES AND NOTES

1. Cui, Y.; Wei, Q.; Park, H.; Lieber, C. M. Nanowire Nanosensors for Highly Sensitive and Selective Detection of Biological and Chemical Species. *Science* **2001**, *293*, 1289–1292.
2. Zheng, G.; Patolsky, F.; Cui, Y.; Wang, W. U.; Lieber, C. M. Multiplexed Electrical Detection of Cancer Markers with Nanowire Sensor Arrays. *Nat. Biotechnol.* **2005**, *23*, 1294–1301.
3. Stern, E.; Klemic, J. F.; Routenberg, D. A.; Wyrembak, P. N.; Turner-Evans, D. B.; Hamilton, A. D.; LaVan, D. A.; Fahmy, T. M.; Reed, M. A. Label-Free Immunodetection with CMOS-Compatible Semiconducting Nanowires. *Nature* **2007**, *445*, 519–522.
4. Hahm, J.; Lieber, C. M. Direct Ultrasensitive Electrical Detection of DNA and DNA Sequence Variations Using Nanowire Nanosensors. *Nano Lett.* **2004**, *4*, 51–54.
5. Bunimovich, Y. L.; Shin, Y. S.; Yeo, W. S.; Amori, M.; Kwong, G.; Heath, J. R. Quantitative Real-Time Measurements of DNA Hybridization with Alkylated Nonoxidized Silicon Nanowires in Electrolyte Solution. *J. Am. Chem. Soc.* **2006**, *128*, 16323–16331.
6. Patolsky, F.; Zheng, G.; Hayden, O.; Lakadamyali, M.; Zhuang, X.; Lieber, C. M. Electrical Detection of Single Viruses. *Proc. Natl. Acad. Sci. U.S.A.* **2004**, *101*, 14017–14022.
7. Minot, E. D.; Janssens, A. M.; Heller, I.; Herring, H. A.; Dekker, C.; Lemay, S. G. Carbon Nanotube Biosensors: The Critical Role of the Reference Electrode. *Appl. Phys. Lett.* **2007**, *91*, 093507–093507-03.
8. Fan, Z.; Lu, J. G. Chemical Sensing with ZnO Nanowire Field-Effect Transistor. *IEEE Trans. Nanotechnol.* **2006**, *5*, 393–396.
9. Li, C.; Curreli, M.; Lin, H.; Lei, B.; Ishikawa, F. N.; Datar, R.; Cote, R. J.; Thompson, M. E.; Zhou, C. Complementary Detection of Prostate-Specific Antigen Using In_2O_3 Nanowires and Carbon Nanotubes. *J. Am. Chem. Soc.* **2005**, *127*, 12484–12485.
10. Zhang, G. J.; Zhang, G.; Chua, J. H.; Chee, R. E.; Wong, E. H.; Agarwal, A.; Buddharaju, K. D.; Singh, N.; Gao, Z.; Balasubramanian, N. DNA Sensing by Silicon Nanowire: Charge Layer Distance Dependence. *Nano Lett.* **2008**, *8*, 1066–1070.
11. Maehashi, K.; Katsura, T.; Kerman, K.; Takamura, Y.; Matsumoto, K.; Tamiya, E. Label-Free Protein Biosensor Based on Aptamer-Modified Carbon Nanotube Field-Effect Transistors. *Anal. Chem.* **2007**, *79*, 782–787.
12. Gao, X. P. A.; Zheng, G.; Lieber, C. M. Subthreshold Regime has the Optimal Sensitivity for Nanowire FET Biosensors. *Nano Lett.* **2010**, *10*, 547–552.
13. Heller, I.; Mannik, J.; Lemay, S. G.; Dekker, C. Optimizing the Signal-to-Noise Ratio for Biosensing with Carbon Nanotube Transistors. *Nano Lett.* **2009**, *9*, 377–382.
14. Lu, M. P.; Hsiao, C. Y.; Lai, W. T.; Yang, Y. S. Probing the Sensitivity of Nanowire-Based Biosensors Using Liquid-Gating. *Nanotechnology* **2010**, *21*, 425505.
15. Stern, E.; Steenblock, E. R.; Reed, M. A.; Fahmy, T. M. Label-Free Electronic Detection of the Antigen-Specific T-Cell Immune Response. *Nano Lett.* **2008**, *8*, 3310–3314.
16. Stern, E.; Vacic, A.; Li, C.; Ishikawa, F. N.; Zhou, C.; Reed, M. A.; Fahmy, T. M. A Nanoelectronic Enzyme-Linked Immunosorbent Assay for Detection of Proteins in Physiological Solutions. *Small* **2010**, *6*, 232–238.
17. Squires, T. M.; Messinger, R. J.; Manalis, S. R. Making it Stick: Convection, Reaction and Diffusion in Surface-Based Biosensors. *Nat. Biotechnol.* **2008**, *26*, 417–426.
18. Kim, D. R.; Zheng, X. Numerical Characterization and Optimization of the Microfluidics for Nanowire Biosensors. *Nano Lett.* **2008**, *8*, 3233–3237.
19. Sheehan, P. E.; Whitman, L. J. Detection Limits for Nanoscale Biosensors. *Nano Lett.* **2005**, *5*, 803–807.
20. Cui, Y.; Duan, X.; Hu, J.; Lieber, C. M. Doping and Electrical Transport in Silicon Nanowires. *J. Phys. Chem. B* **2000**, *104*, 5213–5216.
21. Ford, A. C.; Ho, J. C.; Chueh, Y. L.; Tseng, Y. C.; Fan, Z.; Guo, J.; Bokor, J.; Javey, A. Diameter-Dependent Electron Mobility of InAs Nanowires. *Nano Lett.* **2009**, *9*, 360–365.

22. Black, C. T. Self-Aligned Self Assembly of Multi-nanowire Silicon Field Effect Transistors. *Appl. Phys. Lett.* **2005**, *87*, 163113–163116.
23. Zhang, D.; Liu, Z.; Li, C.; Tang, T.; Liu, X.; Han, S.; Lei, B.; Zhou, C. Detection of NO_2 down to ppb Levels Using Individual and Multiple In_2O_3 Nanowire Devices. *Nano Lett.* **2004**, *4*, 1919–1924.
24. Elfstrom, N.; Juhasz, R.; Sychugov, I.; Engfeldt, T.; Karlstrom, A. E.; Linnros, J. Surface Charge Sensitivity of Silicon Nanowires: Size Dependence. *Nano Lett.* **2007**, *7*, 2608–2612.
25. Elfstrom, N.; Karlstrom, A. E.; Linnros, J. Silicon Nanoribbons for Electrical Detection of Biomolecules. *Nano Lett.* **2008**, *8*, 945–949.
26. Li, Z.; Rajendran, B.; Kamins, T. I.; Li, X.; Chen, Y.; Williams, R. S. Silicon Nanowires for Sequence-Specific DNA Sensing: Device Fabrication and Simulation. *Appl. Phys. A: Mater. Sci. Process.* **2005**, *80*, 1257–1263.
27. Nair, P. R.; Alam, M. A. Design Considerations of Silicon Nanowire Biosensors. *IEEE Trans. Electron Devices* **2007**, *54*, 3400–3408.
28. Nair, P. R.; Alam, M. A. Screening-Limited Response of Nanobiosensors. *Nano Lett.* **2008**, *8*, 1281–1285.
29. Heo, K.; Cho, E.; Yang, J.-E.; Kim, M.-H.; Lee, M.; Lee, B. Y.; Kwon, S. G.; Lee, M.-S.; Jo, M.-H.; Choi, H.-J.; *et al.* Large-Scale Assembly of Silicon Nanowire Network-Based Devices Using Conventional Microfabrication Facilities. *Nano Lett.* **2008**, *8*, 4523–4527.
30. Rao, S. G.; Huang, L.; Setyawan, W.; Hong, S. Nanotube Electronics: Large-Scale Assembly of Carbon Nanotubes. *Nature* **2003**, *425*, 36–37.
31. Lee, M.; Im, J.; Lee, B. Y.; Myung, S.; Kang, J.; Huang, L.; Kwon, Y. K.; Hong, S. Linker-Free Directed Assembly of High-Performance Integrated Devices Based on Nanotubes and Nanowires. *Nat. Nanotechnol.* **2006**, *1*, 66–71.
32. Fan, Z.; Ho, J. C.; Jacobson, Z. A.; Yerushalmi, R.; Alley, R. L.; Razavi, H.; Javey, A. Wafer-Scale Assembly of Highly Ordered Semiconductor Nanowire Arrays by Contact Printing. *Nano Lett.* **2008**, *8*, 20–25.
33. Javey, A.; Nam, S.; Friedman, R. S.; Yan, H.; Lieber, C. M. Layer-by-Layer Assembly of Nanowires for Three-Dimensional, Multifunctional Electronics. *Nano Lett.* **2007**, *7*, 773–777.
34. Fan, Z.; Ho, J. C.; Takahashi, T.; Yerushalmi, R.; Takei, K.; Ford, A. C.; Chueh, Y.-L.; Javey, A. Toward the Development of Printable Nanowire Electronics and Sensors. *Adv. Mater.* **2009**, *21*, 3730–3743.
35. Huang, Y.; Duan, X.; Wei, Q.; Lieber, C. M. Directed Assembly of One-Dimensional Nanostructures into Functional Networks. *Science* **2001**, *291*, 630–633.
36. Raychaudhuri, S.; Dayeh, S. A.; Wang, D.; Yu, E. T. Precise Semiconductor Nanowire Placement through Dielectrophoresis. *Nano Lett.* **2009**, *9*, 2260–2266.
37. Lao, C. S.; Liu, J.; Gao, P.; Zhang, L.; Davidovic, D.; Tummala, R.; Wang, Z. L. ZnO Nanobelt/Nanowire Schottky Diodes Formed by Dielectrophoresis Alignment Across Au Electrodes. *Nano Lett.* **2006**, *6*, 263–266.
38. Gao, Z.; Agarwal, A.; Trigg, A. D.; Singh, N.; Fang, C.; Tung, C. H.; Fan, Y.; Buddharaju, K. D.; Kong, J. Silicon Nanowire Arrays for Label-Free Detection of DNA. *Anal. Chem.* **2007**, *79*, 3291–3297.
39. Hu, Y.; Zhou, J.; Yeh, P.-H.; Li, Z.; Wei, T.-Y.; Wang, Z. L. Supersensitive, Fast-Response Nanowire Sensors by Using Schottky Contacts. *Adv. Mater.* **2010**, *22*, 3327–3332.
40. Barzola-Quiquia, J.; Dusari, S.; Bridoux, G.; Bern, F.; Molle, A.; Esquinazi, P. The Influence of Ga(+) Irradiation on the Transport Properties of Mesoscopic Conducting Thin Films. *Nanotechnology* **2010**, *21*, 145306.
41. Gruner, G. Carbon Nanotube Transistors for Biosensing Applications. *Anal. Bioanal. Chem.* **2006**, *384*, 322–335.
42. Stern, E.; Wagner, R.; Sigworth, F. J.; Breaker, R.; Fahmy, T. M.; Reed, M. A. Importance of the Debye Screening Length on Nanowire Field Effect Transistor Sensors. *Nano Lett.* **2007**, *7*, 3405–3409.
43. Hermanson, G. T. In *Bioconjugate Techniques*, 2nd ed.; Academic Press: New York, 2008.